JOURNAL OF OPTOELECTRONICS AND ADVANCED MATERIALS Vol. 8, No. 3, June 2006, p. 1200 - 1205

Ferromagnetic ordering of Mn diluted into InAs(100) probed by x-ray magnetic circular dichroism

C. M. TEODORESCU*, M. C. RICHTER[a], K. HRICOVINI[a]
National Institute of Materials Physics, Atomistilor 105b, Magurele P. O. Box MG7, 077125 Romania
[a]*Laboratoire de Physique des Matériaux et des Surfaces, Université de Cergy-Pontoise, 95031 Cergy-Pontoise France*

This work reports ferromagnetic ordering of manganese atoms diluted into InAs(100), as seen by X-ray magnetic circular dichroism (XMCD). Room-temperature grown Mn layers on InAs(100) are not magnetic, whereas upon annealing at 250 °C, Mn migrates into the semiconductor and exhibits a clear XMCD signal. The net ordered Mn magnetic moment is found to be about 0.7 $_B$ at low temperatures, whereas the Mn atoms are in a state characterized by a local spin of about 2 $_B$. The temperature dependence of the Mn net magnetic moment gives a Curie temperature of more than 150 K, which is higher than the values reported so far for (In,Mn)As and (Ga, Mn)As diluted magnetic semiconductors.

(Received March 20, 2006; accepted May 18, 2006)

Keywords: Diluted magnetic semiconductors, Manganese, Indium arsenide, X-ray magnetic circular dichroism, X-ray absorption

1. Introduction

Magnetic properties of 3*d* transition metals grown on semiconductors have attracted special interest over the last two decades, owing to the possibility of combining magnetism and semiconductor properties and offering a wide range of possible applications [1]. Of these structures, Fe/GaAs [2] and Fe/InAs [3,4] were extensively studied in terms of their interface reaction and magnetism, exploring the possibility of spin injection of carriers into semiconductors [5,6]. Another important attention was given to the growth and characterization of diluted magnetic semiconductors (DMS) $Ga_xMn_{1-x}As$ [7-10] and $In_xMn_{1-x}As$ [10-13] because it appears that the spin injecton efficiency increase when spins are provided by a semiconducor instead of a metal [6,14, 15]. However, such "all-semiconductor" spintronic devices [6,16] are not yet operational at room temperature due to the relative low Curie temperatures (T_C) of the DMS known to date: about 110 K for (Ga,Mn)As [9] and about 30 K for (In,Mn)As [13]. It appears therefore that more effort is needed in order to increase T_C of these magnetic heterostructures. Multilayer structures with increased T_C [17], "digital heterostructures" [18], as well as new DMS such as (In,Ga,Mn)As [19] or GaMnP [20] have been proposed. In parallel, intensive theoretical studies of the carrier-induced ferromagnetism (FM) in DMS [21-23] yielded predictions on the upper limits of T_C for these materials [22,23]. The key result of these investigations is that in order to achieve higher Curie temperature a higher concentration of magnetic ions and/or carriers (holes) in the material are needed [23]. Whereas the carrier concentration can be externally supplied by light irradiation [24] or electric carrier injection [25], the concentration of Mn ions is limited by the solubility of Mn into the semiconductor with respect to the segregation of MnAs clusters [11,12,26].

Structural studies of (In,Mn)As [26] and (Ga,Mn)As [27] have revealed the local order around the Mn atoms. It is found that Mn atoms occupy mostly substitutional Ga or In sites, with increased disorder induced by the longer Mn-As bonds. Further studies are needed, however, to clarify the atomic magnetic properties of Mn diluted into these semiconductor lattices [28].

X-ray magnetic circular dichroism (XMCD) [29] is the appropriate technique to investigate these properties, since: (i) it is element-sensitive; (ii) it provides quantitatively the local spin and orbital magnetic moments through the application of the sum rules [30,31]; (iii) the detection by total electron yield (TEY) [4,32] in the soft x-ray regime makes the technique surface-sensitive, owing to the finite escape depth of the detected electrons ($\lambda \approx 20$ Å [4,33]). Previous XMCD studies of the (Ga,Mn)As DMS revealed that about 13 % of the Mn atoms present ferromagnetic ordering for temperatures below 37 K, while they are in a high-spin state with local magnetic moment of 4.6 μ_B per Mn atom [34].

In this work, we investigated the magnetic properties of Mn atoms diluted into InAs by XMCD. We present results obtained on (Mn,In)As thin layers prepared in a very simple way, i.e. just by Mn deposition on heated InAs(100) substrates. Ferromagnetic ordering of an important part of Mn atoms is directly experienced for temperatures below 150 K.

2. Experimental

The experiments were performed at the LURE synchrotron radiation laboratory in Orsay, France. We used a molecular beam epitaxy (MBE) chamber equipped with standard surface preparation techniques, LEED, RHEED (low energy- and reflectance high energy electron diffraction), and Auger electron spectroscopy (AES) facilities. The MBE chamber was connected to a "very-low-temperatures" (VLT) measurement chamber, where

samples can be measured at temperatures as low as 1.5 K and in magnetic fields up to 7 T. The whole system was installed on the SU23 beamline of the Super Aco storage ring, which provides photons in the energy range 80-1300 eV with 60 % degree of circular polarisation. The XMCD measurements were performed by recording the TEY signal from the sample when excited with soft x-rays. The in-vacuum sample transfer was achieved by using a specially designed system [35]. The MBE and VLT chambers operate in 10^{-11} hPa pressure range.

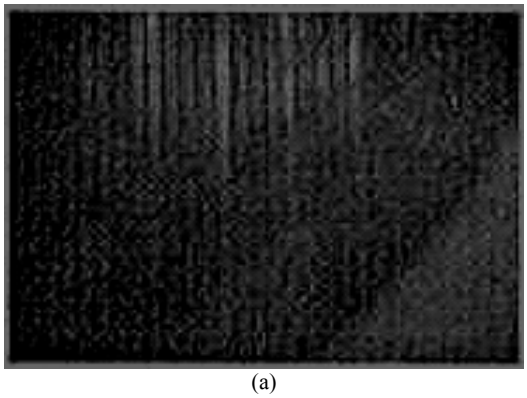

(a)

(b)

Fig. 1. RHEED pattern of (a) clean InAs(100) c(2x4) and (b) of annealed 2 ML Mn/InAs(100).

InAs(100) *c* (2x4) substrates were prepared by Ar^+ sputtering and annealing at 450 ºC. A sharp RHEED pattern of the clean samples was observed on the clean samples [3,4], as can be seen from Fig. 1(a). Manganese was deposited from a commercial Knudsen cell at a rate of about 1 Å/min. The total amount of Mn deposited was in the range of 2 to 3 ML. The samples were checked by AES and no trace of contaminants was visible. Upon Mn deposition at room temperature, the RHEED pattern dissapeared, so these Mn films are disordered. These RT prepared samples did not show any XMCD signal, indicating that no net FM order of the Mn atoms is present. The samples grown at higher substrate temperatures T_S = 250 ºC exhibit a strongly reduced Mn AES (LMM) peak. The effective Mn coverage determined by AES is 0.2 ± 0.1 atomic monolayers (ML). A broad (1x1) RHEED pattern was still visible upon Mn deposition, showing a relatively ordered interface, as exemplified in Fig. 1(b). Samples prepared in a similar manner for surface-sensitive photoemission with photon energy of 85 eV in a separate experiment at the synchrotron ELETTRA in Trieste did not found any Mn 3*p* (binding energy = 47.2 eV) contribution [36]. Consequently, Mn atoms diffuse into the InAs substrate such that a very small amount of Mn (< 0.02 ML) remain in the first atomic layers probed in the photoemission experiment. The growth temperature was chosen to be high enough to allow the diffusion of Mn atoms into the substrate, but to prevent segregation of MnAs clusters [11,26], which are known to be formed at higher substrate temperatures (T_S > 280 ºC [11]).

3. Results and discussion

The high-temperature grown samples presented Mn $L_{2,3}$ XMCD signals, as shown in Fig. 2(a). The two x-ray absorption spectra (XAS) are measured in applied magnetic fields parallel to the helicity of the soft x-rays $H = \pm 5$ T and at 45 degrees incidence angle. The sample was mounted with the [110] direction horizontal, such that the incidence direction of the photon beam corresponds to the [111] axis. The high value of the applied field ensures that the sample magnetisation is saturated, as can be seen from the insert of Fig. 2(a).

The two main peaks correspond to the $L_{2,3}$ absorption, promoting a Mn $2p_{3/2}$ or $2p_{1/2}$ core electron mainly into unoccupied 3*d* states. The absorption signals $\sigma_{+,-}$ are different when the sample magnetization is parallel or antiparallel to the helicity vector of the circularly-polarized x-rays.

The XAS can be also used to determine the Mn dilution into the InAs. The relevant parameter in this case is the ratio between the L_3 maximum intensity (*P*) and the background (*B*): $P/B - 1 = \sigma(L_3) / \sigma_B - 1$. Here $P/B - 1 = 0.83$, whereas for 0.5 ML Mn/Cu(100) $P/B - 1 = 0.243$ [37] and for 1 ML Mn/Fe(100) $P/B - 1 \approx 0.5$ [38], i.e. $P_0/B_0 - 1 \approx 0.5$ for 1 ML of Mn independent of the substrate used, provided no absorption edge lies just before the Mn $L_{2,3}$ edges. The probing depth of the TEY technique is $\lambda = 20$ Å ≈ 14 ML of Mn [33]. The effective Mn concentration is thus estimated as $(P/B - 1)/[(P_0/B_0 - 1)\lambda(\mathrm{ML})] \approx 11.8$ % in a thickness range of λ, which is consistent with the AES estimates. Nevertheless, the absence of Mn 3*p* signal in surface-sensitive PES means that Mn atoms have migrated deeper into the substrate [39].

The difference between the two XAS spectra represents the dichroism signal $\mu = \sigma_+ - \sigma_-$, which is proportional to the Mn net magnetic moment. Theory predicts that spin and orbital magnetic moments can be derived by using the XMCD sum rules, in the following way [30,31]: from the net isotropic absorption spectrum, a double step background accounting for $2p \rightarrow ns, nd$ ($n \geq 4$) and $2p \rightarrow$ continuum transitions is subtracted, in order to isolate the $2p_{3/2} \rightarrow 3d$ and $2p_{1/2} \rightarrow s\ 3d$ absorption cross section for the two polarizations $\sigma_+^{(0)}$ and $\sigma_-^{(0)}$. The

average spectrum $\sigma^{(0)} = [\sigma_+^{(0)} + \sigma_-^{(0)}]/2$ is then integrated, yielding the parameter:

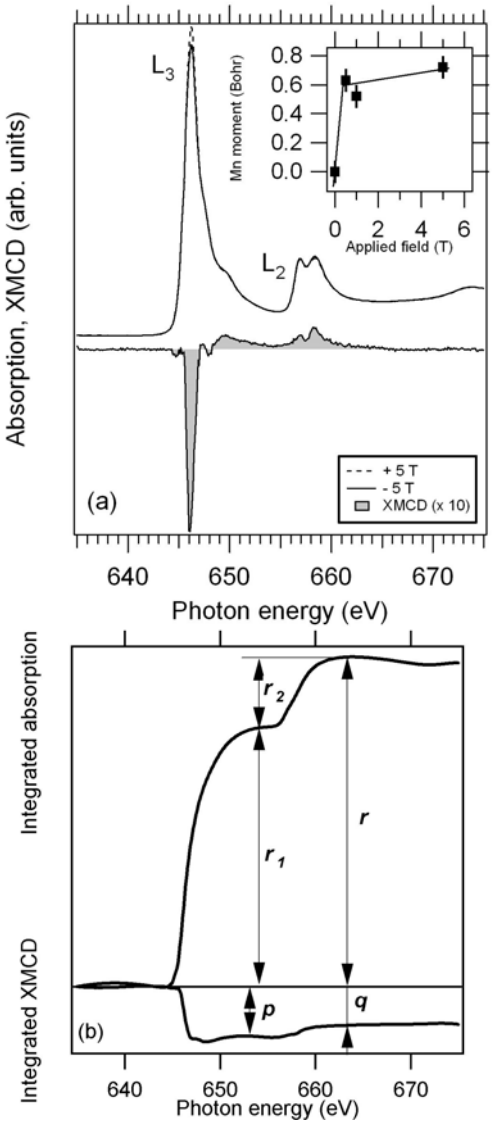

Fig. 2.(a) Mn $L_{2,3}$ x-ray absorption and x-ray magnetic circular dichroism recorded at a temperature of 4.2 K and in applied field H =± 5 T. Insert: the dependence of the Mn magnetic moment on the intensity of the applied field. (b) Integrated isotropic absorption and XMCD, in order to reveal the significance of the p, q, r, r_1, r_2 parameters.

$$r = \int_{L_3+L_2} \sigma^{(0)} dE = r_1 + r_2 \qquad (1)$$

The XMCD spectrum μ is also integrated for the computation of the other two parameters needed by the sum rules:

$$p = \int_{L_3} \mu \cdot dE \text{ and } q = \int_{L_3+L_2} \mu \cdot dE \qquad (2)$$

Integrals of isotropic absorption and of XMCD, together with the significance of parameters defined by the above equations, are represented in Fig. 2(b).

The orbital and spin magnetic moments are derived as $m_{orb.} = -2q\, n_h / (3r)$ and $m_{spin} = (2q - 3p)\, n_h / r$, where n_h is the number of Mn 3*d* holes, which is estimated to about 4.8 for $Ga_xMn_{1-x}As$ from photoemission experiments [40] and to 4.77 from XMCD experiments [41].

Next, we investigated the temperature dependence of the Mn magnetic moments. As can be seen from Fig. 3, detectable XMCD signals were provided by the prepared samples up to temperatures of about 120 K.

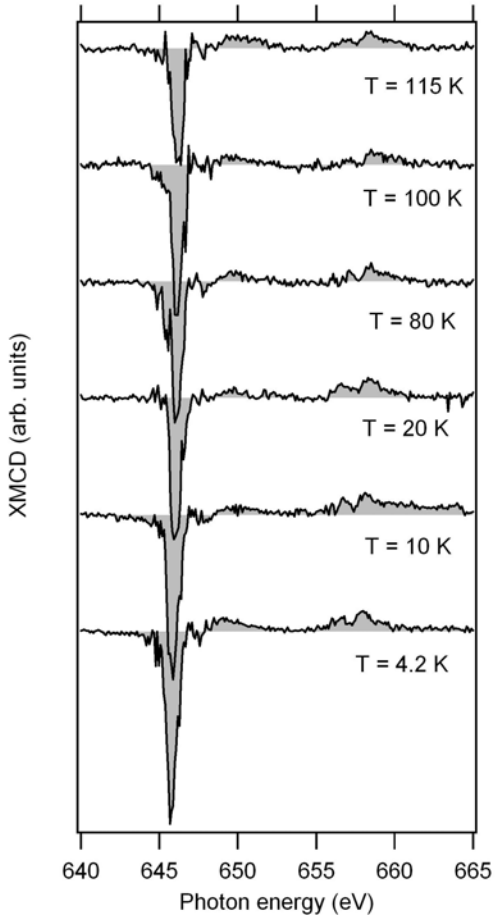

Fig. 3. Dependence of XMCD signal of ≈ 12 % Mn diluted into InAs(100) on temperature.

It is often argued that the XMCD sum rules are not valid in the case of Mn, due to the small spin-orbit splitting and the mixing of the electronic transitions at the $L_{2,3}$ edges [38,42]. Consequently, the spin sum rule may yield wrong results through the insufficient determination of the *p* parameter. However, in the following we will suppose that the *orbital* sum rule is still valid, since it is based on integration over *both* $L_{2,3}$ edges [34]. Instead of

the spin sum rule, we will estimate the total Mn momentum by direct comparison of the normalized L_3 XMCD intensity $s = \mu(L_3^{(max.)}) / \sigma^{(0)}(L_3^{(max.)})$ with known data already reported in literature [37]. For 1 μ_B of Mn magnetic moments, reported values of s were 8.8 % [43], 9.2 % [38], 8.5 % [44], and 12.6 % in the case of oxidized Mn/Fe(100) [41], but in the last case the overall XMCD spectrum was different due to antiferromagnetic coupling of Mn moments to the Fe moments [45]. Consequently, we will assume that a FM Mn XMCD signal of s = 8.8 % corresponds to 1 μ_B [37].

The orbital and total moments derived by XMCD sum rules are compared with the total moment estimated from the intensity of the XMCD signal at the L_3 edge*s* in Fig. 3 (see below). We found that the sum rule underestimates the Mn magnetic moment by a factor of 2. In other words, the estimated p parameter is in the following relation with the "ideal" one p_0: $p = p_0/2 + q/3$, provided the q value is correct.

Fig. 4 presents the temperature dependence of the Mn magnetic moments. We observed a clear XMCD signal up to temperatures of 140 K, then the signal drops rapidly to zero. The temperature dependence of Mn atomic moments was compared with FM curves obtained by solving the Brillouin equation with different values of individual spins [46]. Although the scattering of the data is too large in order to derive precisely the value of the Mn spin moment S, it seems that the function with S = 1 describes better the $M(T)$ dependence than the function with S = 5/2. In all cases, the critical temperature for FM ordering is found to be at 150-160 K, which is the highest value reported so far for Mn in InAs.

Regarding the individual Mn spin moments, we can also specify that the branching ratio (BR) of integrated intensities $I(L_3) / I(L_2) = r_1 / r_2$, according to Fig. 1(b), was found to be 3.26 ± 0.1, independent on the applied magnetic field and/or the temperature. Values of BR can be as high as 4.1 [44] or even 4.8 [47] for high-spin Mn states with individual spin moments of 5 μ_B, whereas for low spin states Mn^{3+} ($4s^2 3d^1$) or Mn^{4+} ($4s^1 3d^1$) with 3d moments of 1 μ_B, it is found to be around 2.5 [44]. Taking into account the above, the actual value of the Mn spin which can be derived by linear interpolation ranges between 1.6 and 2.4 μ_B, which mean an average value of S = 1 (m_{spin} = 2 μ_B), in line with the effective moment dependence on temperature represented in Fig. 4. Hence, the Mn atoms are not in extremely high spin moment state, as in the case of other Mn thin films [44,47]. Nevertheless, the effective moment of about 0.72 μ_B implies that about a third part of Mn spins produce a net ferromanetic moment. Hence, a prospective representation of Mn states would be a *ferrimagnetic* ordering on the type: ↑↓↑↑↓↑↑↓↑...

At low temperature, deviations from the Brillouin dependence of $M(T)$ are present. These were simulated in Fig. 4 by adding a linear component at very low temperatures $\Delta M = 1 - a \times T$. Such dependencies can be attributed to a surface spin wave contribution to the magnetisation [21,28,48]. In fact, the temperature dependence of the magnetization was predicted to have various shapes, deviating considerably from the mean-field dependence [48]. Similar almost linear dependencies were already reported for both (Ga,Mn)As [8,49] and (In,Mn)As DMS [12].

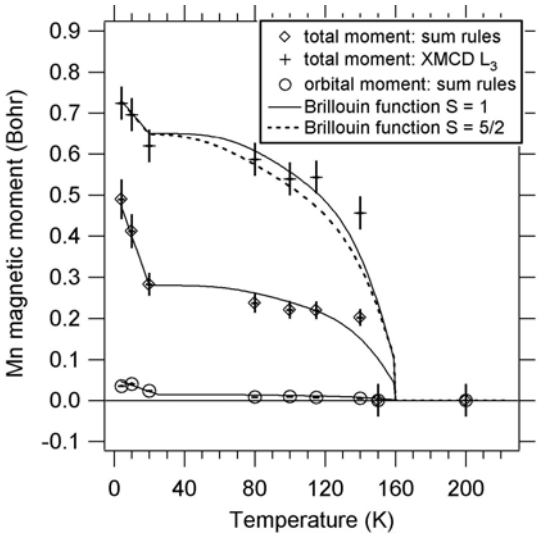

Fig. 4. Temperature dependence of the Mn total and orbital moments, obtained from XMCD data recorded at fields of ± 5 T. For the total moment, the value obtained from the XMCD intensity at the L_3 peak energy is compared with the value derived by the applications of XMCD orbital and spin sum rules (see text for details).

The orbital moment is normally strongly enhanced at the surfaces [50] and at interfaces between 3d metals and III-V semiconductors [4,51]; however, this is not the case here. The Mn orbital moments derived by the XMCD sum rule are very weak: 0.035-0.04 ± 0.005 μ_B at low temperatures, up to 0.007 ± μ_B at 140 K. The ratio between the orbital and the spin moment approaches that of the bulk ferromagnets Fe, Co, and Ni [31]. This is similar to the known orbital momentum quenching in cubic crystal lattices [52] and could be interpreted as another evidence of the strong diffusion of Mn into InAs and of cubic, bulklike environment of the Mn atoms.

4. Conclusions

Mn atoms diluted into InAs(100) by simple deposition at high temperature T_S = 250 ºC present feromagnetic ordering with Curie temperature of about 150 K and are in an intermediate-spin state, characterized by an atomic Mn moment of about 2 μ_B. About one third of Mn atoms participate to the FM order. The Mn effective magnetic moment is found to be 0.7 μ_B at low temperatures and follows a Brillouin dependence as function of temperature when approaching T_C, whereas at low temperatures we found deviations from this dependence which could be explained by surface spin excitations. The orbital moment of Mn is very weak, about 0.04 μ_B. Previous studies of x-ray absorption fine structure on (In,Mn)As [26] always inferred substitution of In by Mn in the present Mn

concentration range. Taking into account that no FM signal which could be attributed to MnAs agglomerates was measured in the present experiment, we could think that Mn atoms are in a similar environment as in DMS (In,Mn)As. However, more precise determination of Mn concentration profile and of the Mn local structure are needed; these experiments are planned for the future.

Acknowledgements

Supports from the Romanian Ministry of Education and Research through Contracts CERES No. 4-40/2004 and CEX05-D11-32/2005 are gratefully acknowledged.

References

[1] G. A. Prinz, Science **250**, 1092 (1990); *ibid.* **282**, 1660 (1998); G. A. Prinz, J. Magn. Magn. Mat. **200**, 57 (1999).

[2] M. W. Ruckman, J. J. Joyce, J. H. Weaver, Phys. Rev. B **33**, 7029 (1986); S. A. Chambers, F. Xu, H. W. Chen, I. M. Vitomirov, S. B. Anderson, J. H. Weaver, Phys. Rev. B **34**, 6605 (1986); J. J. Krebs, B. T. Jonker, G. A. Prinz, J. Appl. Phys. **61**, 2596 (1987); G. W. Anderson, M. C. Hanf, P. R. Norton, Phys. Rev. Lett. **74**, 2764 (1995); A. Filipe, A. Schuhl, P. Galtier, Appl. Phys. Lett. **70**, 129 (1997); B. Lépine, S. Ababou, A. Guivarc'h, G. Jézequel, S. Députier, R. Guérin, A. Filipe, A. Schuhl, F. Abel, C. Cohen, A. Rocher, J. Crestou, J. Appl. Phys. **83**, 3077 (1998); Y. B. Xu, E.T.M. Kernohan, D. J. Freeland, A. Ercole, M. Tselepi, J. A. C. Bland, Phys. Rev. B **58**, 890 (1998).

[3] Y. B. Xu, E. T. M. Kerhohan, M. Tselepi, J. A. C. Bland, S. Holmes, Appl. Phys. Lett. **73**, 399 (1998); Y. B. Xu, D. J. Freeland, M. Tselepi, J. A. C. Bland, Phys. Rev. B **62**, 1167 (2000); M. Tselepi Y. B. Xu, D. J. Freeland, T. A. Moore, J. A. C. Bland, J. Magn. Magn. Mat. **226-230**, 1585 (2001); C. Teodorescu, F. Chevrier, V. Ilakovac, O. Heckmann, L. Lechevalier, R. Brochier, R. L. Johnson, K. Hricovini, Appl. Surf. Sci. **166**, 137 (2000); C. M. Teodorescu, F. Chevrier, R. Brochier, C. Richter, O. Heckmann, V. Ilakovac, P. De Padova, K. Hricovini, Surf. Sci. **482-485**, 1004 (2001).

[4] C. M. Teodorescu, F. Chevrier, R. Brochier, V. Ilakovac, O. Heckmann, L. Lechevalier, K. Hricovini, Eur. Phys. J. B **28**, 305 (2002).

[5] M. Johnson, R. H. Silsbee, Phys. Rev. B **37**, 5312 and 5326 (1988); S. Datta, B. Das, Appl. Phys. Lett. **56**, 665 (1990); M. Johnson, Science **260**, 320 (1993); M. Johnson, J. Magn. Magn. Mat. **140-144**, 21 (1995).

[6] Y. Ohno, D. K. Young, B. Beschoten, F. Matsukura, H. Ohno, D. D. Awschalom, Nature **402**, 790 (1999); M. Yamanouchi, D. Chiba, F. Matsukura, H. Ohno, Nature **428**, 539 (2004).

[7] H. Ohno, A. Shen, F. Matsukura, A. Oiwa, A. Endo, S. Katsumoto, Y. Iye, Appl. Phys. Lett. **69**, 363 (1996).

[8] B. Beschoten, P. A. Crowell, I. Malajovich, D. D. Awschalom, F. Matsukura, A. Shen, H. Ohno, Phys. Rev. Lett. **83**, 3073 (1999).

[9] F. Matsukura, H. Ohno, A. Shen, Y. Sugawara, Phys. Rev. B **57**, R2037 (1998).

[10] H. Ohno, Science **281**, 951 (1998); H. Ohno, J. Magn. Magn. Mat. **200**, 110 (1999).

[11] H. Munekata, H. Ohno, S. Von Molnár, A. Segmuller, L. L. Chang, L. Esaki, Phys. Rev. Lett. **63**, 1849 (1989); H. Munekata, H. Ohno, S. Von Molnár, A. Harwit, A. Segmuller, L. L. Chang, J. Vac. Sci. Technol. B **8**, 176 (1990).

[12] H. Ohno, H. Munekata, S. Von Molnár, L. L. Chang, J. Appl. Phys. **69**, 6103 (1991); H. Ohno, H. Munekata, T. Penney, S. Von Molnár, L. L. Chang, Phys. Rev. Lett. **68**, 2664 (1992).

[13] H. Munekata, A. Zaslavsky, P. Fumagalli, R. J. Gambino, Appl. Phys. Lett. **63**, 2929 (1993).

[14] G. Borghs, J. DeBoeck, Mater. Sci. Eng. B **84**, 75 (2001).

[15] H. J. Zhu, M. Ramsteiner, H. Kostial, M. Wassermeier, H. P. Schonherr, K. H. Ploog, Phys. Rev. Lett. **87**, 016601 (2001).

[16] H. Ohno, D. Chiba, F. Matsukura, T. Omiya, E. Abe, T. Dietl, Y. Ohno, K. Ohtani, Nature **408**, 944 (2000).

[17] T. Jungwirth, W. A. Atkinson, B. H. Lee, A. H. MacDonald, Phys. Rev. B **59**, 9818 (1999); D. Chiba, N. Akiba, F. Matsukura, Y. Ohno, H. Ohno, Appl. Phys. Lett. **77**, 1873 (2000); I. Vurgaftman, J. R. Meyer, Phys. Rev. B **64**, 245207 (2001); H. Ohno, F. Matsukura, Y. Ohno, Sol. State Commun. **119**, 281 (2001).

[18] R. K. Kawakami, E. Johnston-Halperin, L. F. Chen, M. Hanson, N. Guebels, J. S. Speck, A. C. Gossard, A. A. Awschalom, Appl. Phys. Lett. **77**, 2379 (2000).

[19] T. Slupinski, H. Munekata, A. Oiwa, Appl. Phys. Lett. **80**, 1592 (2002).

[20] M. E. Overberg, B. P. Gila, C. R. Abernathy, S. J. Pearton, N. A. Theodoropolou, K. T. McCarthy, S. B. Arnason, A. F. Hebard, Appl. Phys. Lett. **79**, 3128 (2001).

[21] T. Dietl, H. Ohno, F. Matsukura, Phys. Rev. B **63**, 195205 (2001).

[22] J. Schliemann, J. Konig, H. H. Lin, A. H. MacDonald, Appl. Phys. Lett. **78**, 1550 (2001); A. Chattopadhyay, S. Das Sarma, A. J. Millis, Phys. Rev. Lett. **87**, 227202 (2001); J. Schliemann, J. Konig, A. H. MacDonald, Phys. Rev. B **64**, 165201 (2001); T. Dietl, H. Ohno, Physica E **9**, 185 (2001).

[23] T. Dietl, H. Ohno, F. Matsukura, J. Cibert, D. Ferrand, Science **287**, 1019 (2000).

[24] S. Koshihara, A. Oiwa, M. Hirasawa, S. Katsumoto, Y. Iye, C. Urano, H. Takagi, H. Munekata, Phys. Rev. Lett. **78**, 4617 (1997); H. Munekata, T. Abe, S. Koshihara, A. Oiwa, M. Hirasawa, S. Katsumoto, Y. Iye, C. Urano, H. Takagi, J. Appl. Phys. **81**, 4862 (1997).

[25] A. Haury, A. Wasiela, A. Arnoult, J. Cibert, S. Tatarenko, T. Dietl, Y. M. d'Aubigné, Phys. Rev. Lett. **79**, 511 (1997).

[26] A. Krol, Y. L. Soo, S. Huang, Z. H. Ming, Y. H. Kao, H. Munekata, L. L. Chang, Phys. Rev. B **47**, 7187 (1993); Y. L. Soo, S. W. Huang, Z. H. Ming, Y. H. Kao, H. Munekata, L. L. Chang, Phys. Rev. B **53**, 4905 (1996); H. Ofuchi, T. Kubo, M. Tabuchi, Y. Takeda, F. Matsukura, S. P. Guo, A. Shen, H. Ohno, J. Appl. Phys. **89**, 66 (2001).

[27] R. Shioda, K. Ando, T. Hayashi, M. Tanaka, Phys. Rev. B **58**, 1100 (1998).

[28] J. Konig, H. H. Lin, A. H. MacDonald, Phys. Rev. Lett. **84**, 5628 (2000).

[29] G. van der Laan, B. T. Thole, G. A. Sawatzky, J. B. Goedkoop, J. C. Fuggle, J. M. Esteva, R. C. Karnatak, Phys. Rev. B **34**, 6529 (1986); G. Schütz, W. Wagner, M. Wilhelm, P. Kniele, R. Zeller, R. Frahm, G. Materlik, Phys. Rev. Lett. **58**, 737 (1987).

[30] B. T. Thole, P. Carra, F. Sette, G. van der Laan, Phys. Rev. Lett. **68**, 1943 (1992); P. Carra, B. T. Thole, M. Altarelli, X. D. Wang, Phys. Rev. Lett. **70**, 694 (1993).

[31] C. T. Chen, Y. U. Idzerda, H. J. Lin, N. V. Smith, G. Meigs, E. Chaban, G. H. Ho, E. Pellegrin, F. Sette, Phys. Rev. Lett. **75**, 152 (1995); C. M. Teodorescu, D. Macovei, A. Lungu, J. Optoelectron. Adv. Mater. **6**, 1275 (2004).

[32] J. M. Esteva, R. C. Karnatak, J. Phys. France **42**, C2-279 (1984).

[33] W. L. O'Brien, B. P. Tonner, Phys. Rev. B **50**, 12672 (1994).

[34] H. Ohldag, V. Solinus, F. U. Hillebrecht, J. B. Goedkoop, M. Finazzi, F. Matsukura, H. Ohno, Appl. Phys. Lett. **76**, 2928 (2000); K. W. Edmonds, N. R. S. Farley, T. K. Johal, G. van der Laan, R. P. Campion, B. L. Gallagher, C. T. Foxton, Phys. Rev. B **71**, 064418 (2005).

[35] C. M. Teodorescu, J. P. Kappler, unpublished.

[36] K. Hricovini, P. De Padova, C. Quaresima, P. Perfetti, R. Brochier, C. Richter, V. Ilakovac, O. Heckmann, L. Lechevalier, P. Bencok, C. Teodorescu, V. Y. Aristov, European Conference on Surface Science ECOSS-19, Madrid, Spetember 5-8 (2000).

[37] Y. Huttel, C. M. Teodorescu, F. Bertrand, G. Krill, Phys. Rev. B **64**, 094405 (2001).

[38] S. Andrieu, E. Foy, H. Fischer, M. Alnot, F. Chevrier, G. Krill, M. Piecuch, Phys. Rev. B **58**, 8210 (1998).

[39] Summarizing the various measurements of the Mn detected coverage θ, as function of the probing depth of each technique (λ): (i) $\theta < 0.02$ ML from surface sensitive PES ($\lambda \approx 2.2$ ML); (ii) $\theta \approx 0.2$ ML from AES ($\lambda \approx 4$ ML); and (iii) $\theta \approx 1.7$ ML from TEY-XAS ($\lambda \approx 14$ ML), this is consistent with a non-uniform distribution of Mn as function of depth. The simplest model, in which d_0 ML at the surface are completely free of Mn, and the Mn concentration, x_0, is constant for deeper layers, give $d_0 \approx 5$ ML and $x_0 \approx 17$ % at. Mn.

[40] J. Okabayashi, A. Kimura, O. Rader, T. Mizokawa, A. Fujimori, Phys. Rev. B **58**, R4211 (1998).

[41] J. Dresselhaus, D. Spanke, F. U. Hillebrecht, E. Kisker, G. van der Laan, J. B. Goedkoop, N. B. Brookes, Phys. Rev. B **56**, 5461 (1997).

[42] P. Turban, S. Andrieu, B. Kierren, E. Snoeck, C. Teodorescu, A. Traerse, Phys. Rev. B **65**, 134417 (2002).

[43] S. Andrieu, M. Finazzi, P. Bauer, H. Fischer, P. Lefevre, A. Traverse, K. Hricovini, G. Krill, M. Piecuch, Phys. Rev. B **57**, 1985 (1998).

[44] W. L. O'Brien, B. P. Tonner, Phys. Rev. B **50**, 2963 (1994); *ibid.* **51**, 617 (1995).

[45] W. L. O'Brien, B. P. Tonner, Phys. Rev. B **58**, 3191 (1998).

[46] C. M. Teodorescu, J. Magn. Magn. Mat., *submitted*.

[47] Y. Huttel, F. Schiller, J. Avila, M. C. Asensio, Phys. Rev. B **61**, 4948 (2000).

[48] J. M. Wesselinowa, E. Kroumova, N. Toefilov, W. Nolting, Phys. Rev. B **57**, 6508 (1998); K. Nishizawa, O. Sakai, S. Suzuki, Physica B **281-282**, 468 (2000); O. Sakai, S. Suzuki, Physica E **10**, 148 (2001); J. M. Wesselinowa, P. Entel, J. Magn. Magn. Mat. **236**, 357 (2001).

[49] K. Takamura, F. Matsukura, Y. Ohno, H. Ohno, J. Appl. Phys. **89**, 7024 (2001); J. Sadowski, R. Mathieu, P. Svedlindh, M. Karlsteen, J. Kanski, L. Iver, H. Åsklund, K. Swiatek, J. Z. Domagala, J. Bak-Misiuk, D. Maude, Physica E **10**, 181 (2001).

[50] O. Eriksson, A. M. Boring, R. C. Albers, G. W. Fernando, B. R. Cooper, Phys. Rev. B **45**, 2868 (1992); M. Tischer, O. Hjortstam, D. Arvanitis, J. Hunter Dunn, F. May, K. Baberschke, J. Trygg, J. M. Wills, B. Johansson, O. Eriksson, Phys. Rev. Lett. **75**, 1602 (1995).

[51] Y. B. Xu, M. Tselepi, C. M. Guertler, C. A. F. Vaz, G. Wastlbauer, J. A. C. Bland, E. Dudzik, G. van der Laan, J. Appl. Phys. **89**, 7156 (2001).

[52] The simplest explanation of orbital momentum quenching can be found in A. Aharoni, *Introduction to the Theory of Ferromagnetism*, Oxford University Press, Oxford (1988): the orbital momentum $\hat{L} = -i\hbar\partial/\partial\phi$, when applied to pure real basis wavefunction, which is the case in a cubic environment, must yield real eigenvalues (since $\hat{L}$ is hermitian) which are necessarily zero.

*Corresponding author: teodorescu@infim.ro